research papers

Quantitative studies of pyrocarbon-coated materials using synchrotron radiation

Poonamlata S. Yadav,* Y. S. Kashyap, Tushar Roy, P. S. Sarkar and A. Sinha

Laser and Neutron Physics Section, Bhabha Atomic Research Centre, Mumbai, India.
E-mail: poonamly@barc.gov.in

Phase-contrast imaging provides enhanced image contrast and is important for non-destructive evaluation of structural materials. In this paper, experimental results on in-line phase-contrast imaging using a synchrotron source (ELETTRA, Italy) for objects required in material science applications are discussed. Experiments have been carried out on two types of samples, pyrocarbon-coated zirconia and pyrocarbon-coated alumina microspheres. These have applications in both reactor and industrial fields. The phase-contrast imaging technique is found to be very useful in visualizing and determining the coating thickness of pyrocarbon on zirconia and alumina microspheres. The experiments were carried out at X-ray energies of 16, 18 and 20 keV and different object-to-detector distances. The results describe the contrast values and signal-to-noise ratio for both samples. A comprehensive study was carried out to determine the thickness of the pyrocarbon coating on zirconia and alumina microspheres of diameter 500 µm. The advantages of phase-contrast images are discussed in terms of contrast and resolution, and a comparison is made with absorption images. The results show considerable improvement in contrast with phase-contrast imaging as compared with absorption radiography.

Keywords: phase-contrast imaging; hard X-rays; synchrotron source; refractive index; signal-to-noise ratio; edge enhancement.

1. Introduction:

High-resolution X-ray imaging of the internal details of materials is of great importance in the field of materials research. Although imaging of high-Z materials is carried out using absorption-based techniques, it cannot be used for imaging of low-Z materials such as carbon fibre, carbon composites, polymers *etc.* as the X-ray absorption is much smaller for such materials (Davis *et al.*, 1995). For this reason, phase-contrast X-ray imaging techniques are being explored all over the world owing to their high-contrast capabilities for soft materials. The phase-contrast imaging technique capitalizes on the fact that, at energies suitable for soft material imaging in the range 10–100 keV, the ratio of the real part (δ) to the imaginary part (β) of the X-ray refractive index (namely δ/β) is near to three orders of magnitude (Wilkins *et al.*, 1996; Wu & Liu, 2003). Hence even if absorption is negligible, very small changes in the real part of the refractive index (phase) results in a large variation in intensity modulation owing to gradients in phase at the edges (Davis *et al.*, 1995; Pogany *et al.*, 1997; Wu & Liu, 2003; Donelly *et al.*, 2006). These gradients in phase-change in the object show up as contrast enhancement of the edges. Unlike conventional absorption-based X-ray imaging, phase-contrast imaging requires particular characteristics in terms of source, source-to-object distance *etc.*

This is due to the requirements of both spatial and temporal coherence. This technique has been used for studying the pyrocarbon (PyC)-coated (typically 40–60 µm) metallic matrix. It also provides a useful tool for estimating the coating thickness, uniformity of the coating *etc.* These kinds of materials are important for the development of advanced reactor fuel pins. In this paper we discuss experimental results on in-line phase-contrast imaging using a synchrotron source (ELETTRA, Italy). We observed edge enhancement in (i) a PyC-coated zirconia sample at the PyC-to-air interface only and not at the Zr-to-PyC interface; (ii) a PyC-coated alumina sample at both alumina-to-PyC and PyC-to-air interfaces.

The results describe the signal-to-noise ratio and contrast values at different object-to-detector distances and different X-ray energies for PyC-coated materials, used in both reactor and industrial applications. We have also determined the coating thickness of PyC on zirconia and alumina microspheres.

2. Methods and mathematical formulations

The effects on propagation of the X-ray wave can be described by the refractive index n, which is a complex quantity (James, 1962; Yadav *et al.*, 2006),

Table 1
Calculation of δ and β for zirconia microspheres coated with PyC.

E (keV)	ZrO_2 (δ)	ZrO_2 (β)	ZrO_2 (δ/β)	C (δ)	C (β)	C (δ/β)
16	3.98253×10^{-6}	5.13023×10^{-8}	77.62868	1.7837×10^{-6}	5.8675×10^{-10}	3039.97
18	2.65212×10^{-6}	2.18219×10^{-7}	12.15348	1.409×10^{-6}	3.5098×10^{-10}	4014.47
20	2.56748×10^{-6}	1.49173×10^{-7}	17.21143	1.1412×10^{-6}	2.2297×10^{-10}	5118.18

Table 2
Calculation of δ and β for alumina microspheres coated with PyC.

E (keV)	Al_2O_3 (δ)	Al_2O_3 (β)	Al_2O_3 (δ/β)	C (δ)	C (β)	C (δ/β)
16	3.15999×10^{-6}	9.48457×10^{-9}	333.172	1.7837×10^{-6}	5.8675×10^{-10}	3039.97
18	2.45693×10^{-6}	5.78526×10^{-9}	424.688	1.409×10^{-6}	3.5098×10^{-10}	4014.47
20	1.98043×10^{-6}	3.80294×10^{-9}	520.763	1.1412×10^{-6}	2.2297×10^{-10}	5118.18

$$n = 1 - \delta - i\beta. \tag{1}$$

The real part δ corresponds to the phase shift owing to scattering, and the imaginary part β corresponds to absorption of the wave,

$$\delta = \left(r_e h^2 c^2 / 2\pi E^2\right) N_0 f_{\mathrm{R}}, \tag{2a}$$

$$\beta = \left(r_e h^2 c^2 / 2\pi E^2\right) N_0 f_{\mathrm{Im}}, \tag{2b}$$

where $r_e = e^2/mc^2 = 2.818 \times 10^{-15}$ m is the electron classical radius, λ is the X-ray wavelength, f_{R} and f_{Im} are the real part and imaginary part, respectively, of the atomic scattering factor (http://www.Physics.nist.gov/PhysRefData/FFast/html/form.html), N_0 is the number of atoms per unit volume, h is Planck's constant and c is the velocity of light.

Now we give a brief calculation of δ and β for zirconia, alumina and carbon. For the different X-ray source energies (E), the values of δ and β have been calculated using (2a) and (2b). Plots of δ and β versus E are shown in Figs. 1 and 2.

It can be seen from Tables 1 and 2 that the ratio δ/β becomes larger with increasing X-ray energy, and δ is several orders of magnitude greater than β for low-Z materials and hard X-rays.

We used the following formulae for calculating the contrast, C (Yadav *et al.*, 2006; Born & Wolf, 1999; Pagot *et al.*, 2005; Hirano & Yamasaki, 2006), and signal-to-noise ratio, S/N

(Born & Wolf, 1999; Pagot *et al.*, 2005), to quantify the edge enhancement in the images,

$$C = \frac{I_{\max} - I_{\min}}{I_{\max} + I_{\min}}, \tag{3}$$

$$S/N = \frac{I_{\max} - I_{\min}}{2^{1/2} \sigma_{\mathrm{backg}}}, \tag{4}$$

where $I_{\max}$ and $I_{\min}$ are the maximum and minimum value, respectively, of the intensity profile across the edge, and σ_{backg} is the standard deviation of the intensity distribution in an area outside of the object.

3. Experimental set-up

The experiment was carried out at the SYRMEP beamline at the ELETTRA synchrotron radiation facility in Trieste, Italy (Arfelli *et al.*, 2000; Menk *et al.*, 2005). ELETTRA, a third-generation synchrotron facility, can run at 2.0 or 2.4 GeV with a maximum ring current of 320 or 140 mA, respectively, which can deliver X-rays ranging from the soft X-ray region to the hard X-ray region. The radiation source results from a bending magnet of the storage ring. The cross-sectional dimensions of the electron bunches circulating in the storage
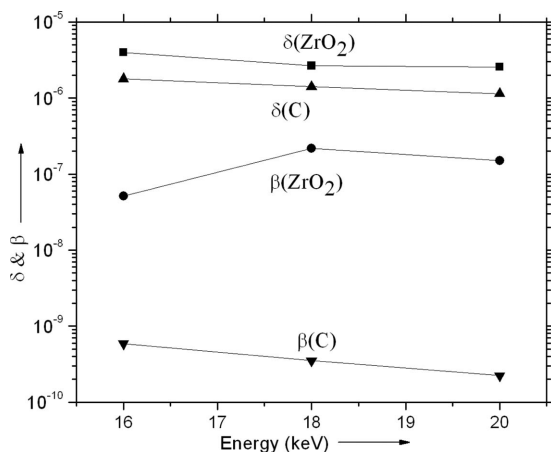

Figure 1
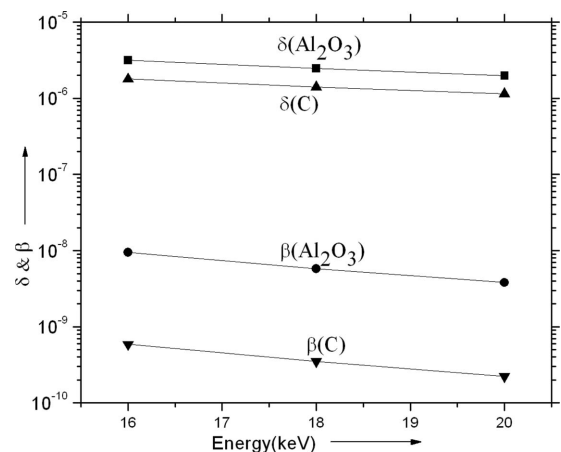Real and imaginary parts (δ and β) of the complex refractive index of zirconia and carbon.

Figure 2
Real and imaginary parts (δ and β) of the complex refractive index of alumina and carbon.

research papers

Table 3
Experimental conditions for sample preparation.

	Temperature (K)	Total flow rate (l m^{-1})	Argon flow rate (l m^{-1})	C$_2$H$_2$ flow rate (l m^{-1})	Time duration (min)
PyC-coated ZrO$_2$ microspheres	1503	15	10	5	30
PyC-coated Al$_2$O$_3$ microspheres	1623	15	11	4	45

Table 4
Comparison of contrast at E = 20 keV using phase and absorption images.

Sample interface	Contrast in phase image	Contrast in absorption
PyC-to-air	0.121	0.0199

Table 5
Comparison of contrast at E = 20 keV using phase and absorption images.

Sample interface	Contrast in phase image	Contrast in absorption
Alumina-to-PyC	0.1851	0.0661
PyC-to-air	0.1459	0.0193

ring are approximately 1100 µm × 140 µm (full width at half-maximum). A monolithic channel-cut Si (111) crystal is used to narrow the energy bandwidth of the incoming white beam. A monochromatic beam, with energy tunable within the range 8–35 keV and an energy resolution of about 0.2%, is thus available in the experimental area. The beamline is characterized by a large source-to-sample distance of 22 m and the object-to-detector distance can be varied up to 1.87 m. A CCD detector and fibre-optic combination having an effective pixel pitch of 4.5 µm was used for collecting high-resolution images.

4. Experimental results and discussion

The coated samples were prepared in a high-temperature graphite vessel. The zirconia and alumina microspheres were spouted using argon gas in the electrically heated graphite vessel. When the desired temperature range (1473–1673 K) is achieved, acetylene gas is passed to deposit PyC. The uniform coating is obtained owing to intimate solid mixing in the spouted bed. We have investigated the characteristics of a PyC coating on zirconia and alumina microspheres prepared under different environmental conditions, as shown in Table 3.

4.1. Case I. Phase-contrast imaging contrast compared with absorption imaging contrast (PyC-coated zirconia microspheres)

Figs. 3(a) and 3(b) show images of a PyC-coated zirconia microsphere of diameter 500 µm. The images were obtained at 20 keV and at a sample-to-detector distance of 50 cm for the

phase-contrast image and 1.8 cm for the absorption image with a scanning time of 4 s. For zirconia, being a high-Z material, the phase variation at the zirconia-to-PyC interface is not highlighted. We calculated the contrast [using (3)] for the PyC-to-air interface. The contrast in the phase-contrast mode is approximately six times greater than that in the absorption mode at the PyC-to-air interface, as shown in Table 4. The thickness of the PyC coating has been determined to be 40 µm for the PyC-coated zirconia microsphere.

4.2. Case II. Phase-contrast imaging contrast compared with absorption imaging contrast (PyC-coated alumina microspheres)

Figs. 4(a) and 4(b) show images of a PyC-coated alumina microsphere of diameter 500 µm. The images were obtained at 20 keV and at a sample-to-detector distance of 50 cm for the phase-contrast image and 1.8 cm for the absorption image with a scanning time of 4 s. We have calculated the contrast [using (3)] for the alumina-to-PyC and PyC-to-air interfaces. The contrast in the phase-contrast image is approximately three times greater than that in the absorption image at the alumina-to-PyC interfaces and approximately eight times at the PyC-to-air interface, as shown in Table 5. In PyC-coated
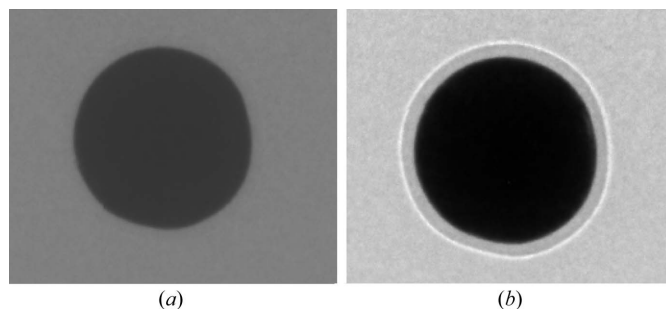

(a)	(b)

Figure 3
(a) Absorption image and (b) phase-contrast image of a PyC-coated zirconia (diameter 500 µm) microsphere acquired at 20 keV. The object-to-detector distances are 1.8 cm and 50 cm, respectively.
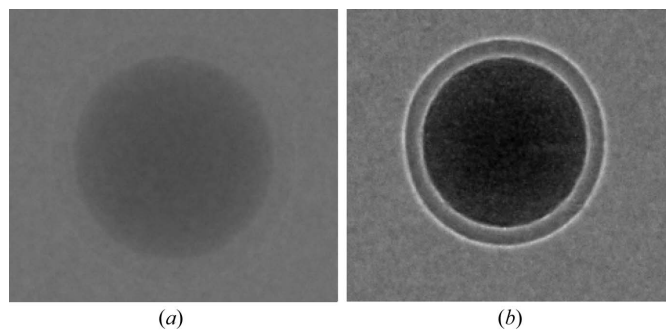

(a)	(b)

Figure 4
(a) Absorption image and (b) phase-contrast image of a PyC-coated alumina (diameter 500 µm) microsphere acquired at 20 keV. The object-to-detector distances are 1.8 cm and 50 cm, respectively.

alumina microspheres the average PyC coating thickness value is 60 µm.

4.3. Case III. Study of contrast and signal-to-noise ratio with object-to-detector distance (PyC-coated zirconia microspheres)

Figs. 5(*a*) and 5(*b*) show the variation of contrast and signal-to-noise ratio, respectively, with the object-to-detector distance using X-ray energy as a parameter. They show the contrast of PyC-coated zirconia microspheres of diameter 500 µm at X-ray energies of 16, 18 and 20 keV and at different object-to-detector distances of 1.8, 15, 35 and 50 cm. We have calculated the contrast and signal-to-noise ratio of the images using equations (3) and (4), respectively, for different object-to-detector distances. We have calculated the contrast at the PyC-to-air interface. The dependence of contrast on the object-to-detector distance is shown in Fig. 5(*a*), from which it is seen that the contrast increases with increasing object-to-detector distance. We can see from Fig. 5(*b*) that the signal-to-noise ratio of the image increases with increasing object-to-detector distance from 1.8 to 50 cm.
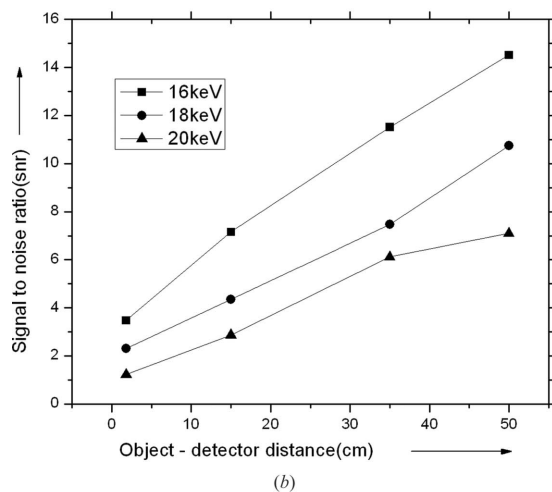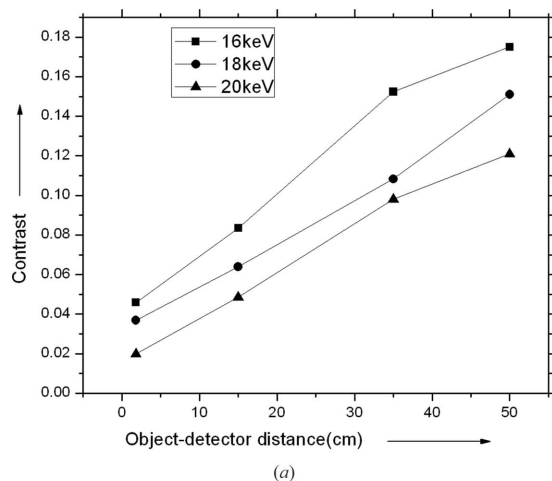
4.4. Case IV. Study of contrast and signal-to-noise ratio with object-to-detector distance (PyC-coated alumina microspheres)

Figs. 6(*a*)–6(*c*) show the variation of contrast and signal-to-noise ratio with object-to-detector distance using X-ray energy as a parameter. They show the contrast of PyC-coated alumina
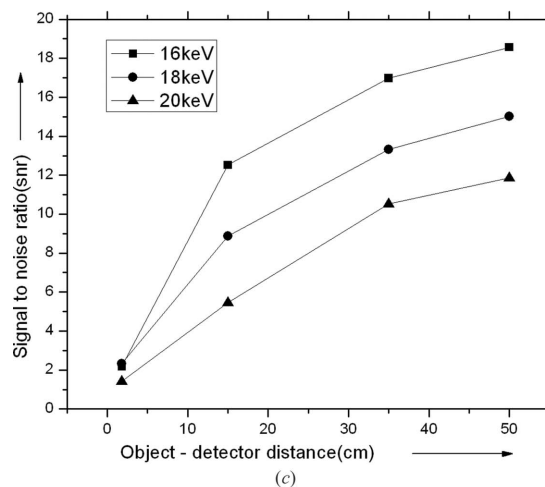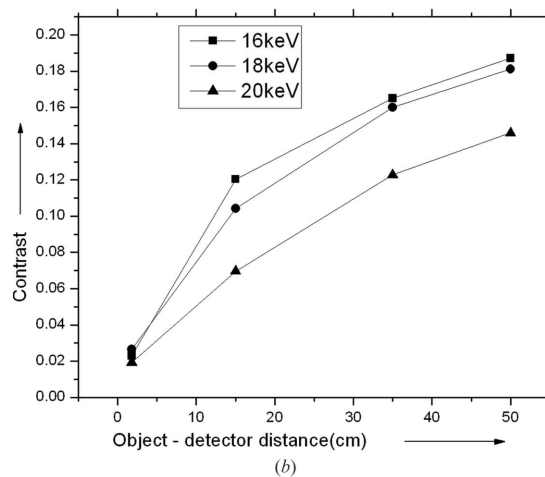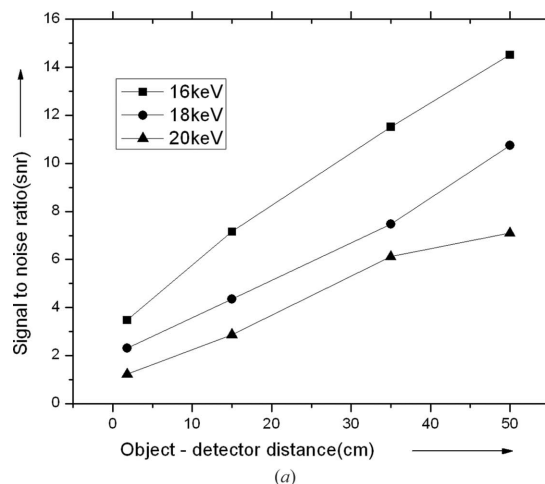

(*a*)

(*b*)

Figure 6
Variation of (*a*) the contrast at the alumina-to-PyC interface, (*b*) the contrast at the PyC-to-air interface and (*c*) the signal-to-noise ratio as a function of the object-to-detector distance at 16, 18 and 20 keV for PyC-coated alumina microspheres.

(*a*)

(*b*)

Figure 5
Variation of (*a*) the contrast and (*b*) the signal-to-noise ratio as a function of the object-to-detector distance at 16, 18 and 20 keV for PyC-coated zirconia microspheres.

(*c*)

microspheres of diameter 500 µm at X-ray energies of 16, 18 and 20 keV and object-to-detector distances of 1.8, 15, 35 and 50 cm. We have calculated the contrast and signal-to-noise ratio of the images using equations (3) and (4) for different object-to-detector distances. The dependence of contrast on the object-to-detector distance is shown in Figs. 6(*a*) and 6(*b*), from which it is seen that the contrast increases with increasing object-to-detector distance. Fig. 6(*c*) shows that the signal-to-noise ratio of the images increases with increasing object-to-detector distance (up to a distance of 50 cm).

4.5. Case V. Study of contrast and signal-to-noise ratio with X-ray energy (PyC-coated zirconia microspheres)

Figs. 7(*a*) and 7(*b*) show the variation of contrast and signal-to-noise ratio with X-ray energy using the object-to-detector distance (1.8, 15, 35 and 50 cm) as a parameter. They show the contrast and signal-to-noise ratio of PyC-coated zirconia microspheres of diameter 500 µm at X-ray energies of 16, 18 and 20 keV. It can be seen that the contrast and signal-to-noise ratio decrease with increasing X-ray energy in the range 16–20 keV.
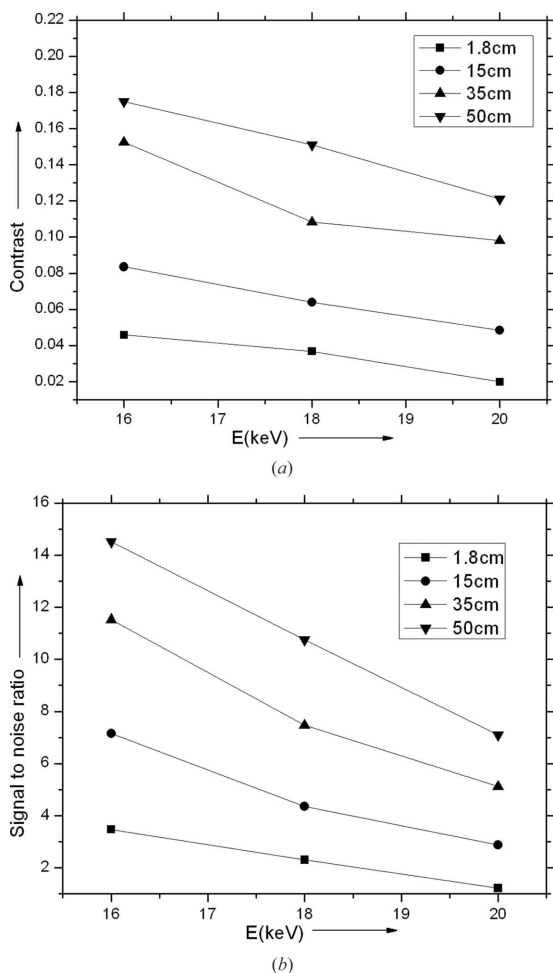
4.6. Case VI. Study of contrast and signal-to-noise ratio with X-ray energy (PyC-coated alumina microspheres)

Figs. 8(*a*)–(*c*) show the variation of contrast and signal-to-noise ratio with X-ray energy using the object-to-detector distance (1.8, 15, 35 and 50 cm) as a parameter. They show the
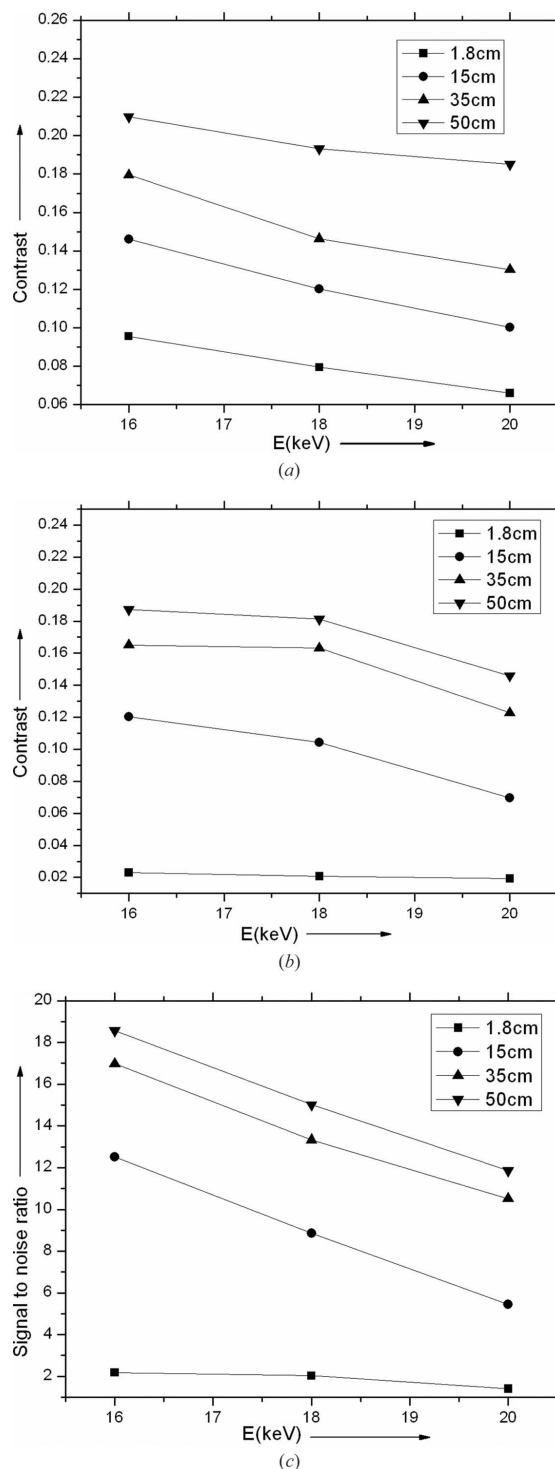

Figure 7
Variation of (*a*) the contrast and (*b*) the signal-to-noise ratio as a function of the X-ray energy at object-to-detector distances of 1.8, 15, 35 and 50 cm for PyC-coated zirconia microspheres.

Figure 8
Variation of (*a*) the contrast at the alumina-to-PyC interface, (*b*) the contrast at the PyC-to-air interface and (*c*) the signal-to-noise ratio as a function of the X-ray energy at sample-to-detector distances of 1.8, 15, 35 and 50 cm for PyC-coated alumina microspheres.

contrast of PyC-coated alumina microspheres of diameter 500 µm at X-ray energies of 16, 18 and 20 keV. It can be seen that the contrast and signal-to-noise ratio decrease with increasing X-ray energy in the range 16–20 keV.

5. Conclusions

In this paper we have discussed our experimental work on X-ray phase imaging to determine the thickness of the PyC coating on zirconia and alumina microspheres using a synchrotron radiation source (ELETTRA, Italy). The coating thickness of PyC was determined to be of the order of 40 µm for zirconia microspheres and of the order of 60 µm for alumina microspheres. We observed edge enhancement in the PyC-coated zirconia microsphere sample at the PyC-to-air interface but not at the zirconia-to-PyC interface, whereas, in the PyC-coated alumina microsphere sample, edge enhancement is observed at both the alumina-to-PyC and PyC-to-air interfaces. We have also calculated the contrast and signal-to-noise ratio for both samples using different X-ray energy and different object-to-detector distances. It is seen that the contrast decreases according to the increase in energy and increases with increasing object-to-detector distance. The signal-to-noise ratio decreases with the increase in energy and increases with increasing object-to-detector distance. The maximum contrast and signal-to-noise ratio was observed at an energy of 16 keV and at an object-to-detector distance of 50 cm.

References

Arfelli, F., Bonvicini, V., Bravin, A. & Cantatore, G. (2000). *Radiology*, **215**, 286–293.

Born, M. & Wolf, E. (1999). *Principles of Optics*, 7th ed. Cambridge University Press.

Davis, T. J., Goa, D., Gureyev, T. E., Stevenson, A. W. & Wilkins, S. W. (1995). *Nature (London)*, **373**, 595–598.

Donelly, E., Lewis, K. G., Wolske, K. M., Pickens, D. R. & Price, R. R. (2006). *Phys. Med. Biol.* **51**, 21–30.

Hirano, M. & Yamasaki, K. (2006). *Nucl. Instrum. Methods Phys. Res. A*, **564**, 496–505.

James, R. W. (1962). *The Optical Principles of the Diffraction of X-rays*, ch. 4. London: Bell & Sons.

Menk, R. H., Rigon, L. & Arfelli, F. (2005). *Nucl. Instrum. Methods Phys. Res. A*, **548**, 213–220.

Pagot, E., Fiedler, S., Cloetens, P. & Bravin, A. (2005). *Phys. Med. Biol.* **50**, 709–724.

Pogany, A., Gao, D. & Wilkins, S. W. (1997). *Rev. Sci. Instrum.* **68**, 2774–2782.

Wilkins, S. W., Gureyev, T. E., Goa, D., Pogany, A. & Stevenson, A. W. (1996). *Nature (London)*, **384**, 335–338.

Wu, X. & Liu, H. (2003). *Med. Phys.* **30**, 2169–2179.

Yadav, P. S., Kashyap, Y., Sarkar, P. S., Sinha, A. & Godwal, B. K. (2006). *Nucl. Instrum. Methods Phys. Res. A*, **564**, 496–505.